RSC Advances

PAPER

View Article Online
View Journal | View Issue

Cite this: *RSC Adv.*, 2017, **7**, 41929

Preparation and properties of poly (lactic acid)/magnetic Fe_3O_4 composites and nonwovens

Bin Yu, *[ab] Mingjun Wang,[ab] Hui Sun,[ab] Feichao Zhu,[ab] Jian Han[ab] and Gajanan Bhat[c]

To develop degradable and magnetic PLA-based melt-blown (MB) nonwoven materials for air filtration applications, poly (lactic acid) (PLA)/magnetic Fe_3O_4 (PLA/Fe_3O_4) MB nonwovens were obtained by melt blowing using the PLA/Fe_3O_4 composites with different components prepared by melt-mixing as the masterbatch. The crystallization and melting behavior of the composites were examined with differential scanning calorimetry (DSC). Although the results showed that the Fe_3O_4 particles obviously hindered the cold crystallization process of PLA and the relative crystallinity degree of the composites decreased due to the addition of Fe_3O_4; there was no overall change in the crystal structure of PLA according to the wide-angle X-ray diffraction (XRD). Thermogravimetric analysis (TGA) and dynamic rheological measurements demonstrated that the introduction of Fe_3O_4 reduced the thermal stability of PLA. The effect of Fe_3O_4 particles on the morphology of the PLA/Fe_3O_4 composites and MB nonwovens was characterized by scanning electron microscopy (SEM). It revealed that the Fe_3O_4 particles were dispersed in a PLA mixture with the "sea-island" structure, and the addition of Fe_3O_4 particles also made the fiber surface rough and the nonwoven web turned fluffy to some extent. The magnetic properties and filtration performance of the MB nonwovens were also investigated in detail.

Received 8th June 2017
Accepted 16th August 2017

DOI: 10.1039/c7ra06427f

rsc.li/rsc-advances

Introduction

With the increasing attention to air filtration materials, melt-blown (MB) nonwoven has drawn people's interest in recent years owning to its highly effective filtration performance and barrier properties.[1,2] Currently, the widely used raw materials for MB nonwovens are polypropylene (PP) and polyethylene terephthalate (PET) but the disposal and subsequent influence on the environment are extremely serious because of their nonbiodegradable nature. Moreover, the eco-friendly bio-based polymers as an answer to the growing sustainability and environmental issues associated with conventional non-biodegradable petroleum-based materials have received increasing interest due to their recyclable, renewable and biodegradable characteristics.[3,4] Thus, a new strategy has emerged to develop bio-based polymer materials for MB nonwoven.[5]

Among many bio-based polymers, poly (lactic acid) (PLA), one of the typical plant-derived biodegradable polymers, can be derived from renewable plant resources (mainly starch and corn or sugar).[6] Owing to its excellent biocompatibility, better thermoplastic processability and reasonably good mechanical properties compared with other bio-derived polymers,[11,12] it shows a tremendous application and huge commercial market prospect for fibers, film materials, and packaging materials.[7–10] Several researchers have focused on the processability and service performance of PLA as a raw material for MB nonwoven;[5,13] the structure and properties of PLA chips and PLA-based blends for melt blowing nonwovens were also analyzed in our previous research.[14,15] All these studies indicated that PLA showed an explosive application prospect in the melt blown nonwoven material.

Melt-mixing process is a rapid method to obtain composite materials; it has the advantages of high production efficiency, less pollution and simple operation. Composting PLA with functionalized inorganic nanofillers by melt-mixing not only presents a simple but effective way to improve the properties of PLA matrix but also endows some added functionalities, such as impressive electrical conductivity, antimicrobial activity, and gas barrier properties,[16–21] which open a promising development and application area of PLA. Ferroferric oxide (Fe_3O_4) as one of the functional materials has been widely used in microwave absorbing materials, catalyst carriers and biomedical fields due to its superior magnetic responsiveness, low toxicity and biocompatibility.[22–26] Interestingly, though there are some studies have demonstrated the PLA based Fe_3O_4 composite prepared by the solution-mixing method and the usage were almost for biomaterials,[27–30] little research has

[a]*The Key Laboratory of Industrial Textile Materials and Manufacturing Technology, Zhejiang Sci-Tech University, Hangzhou, Zhejiang Province, China. E-mail: yubnin7712@163.com; Tel: +86 13758241604*

[b]*School of Materials and Textiles, Zhejiang Sci-Tech University, Hangzhou, China*

[c]*Department of Textiles, Merchandising & Interiors, University of Georgia, Athens, GA 30602, USA*

studied the PLA/Fe_3O_4 composites prepared by melt-mixing and the influence of magnetic Fe_3O_4 on the filtration property of PLA MB nonwoven materials.

In our study, we have hoped to provide some original data for the development of degradable and functional PLA-based MB nonwoven materials for air filtration application. Therefore, magnetic PLA/Fe_3O_4 MB nonwoven materials were fabricated by melt-blowing processing using the PLA/Fe_3O_4 composites as the raw materials that were prepared and pelletized by melt-mixing. Some correlative performances were characterized to evaluate the influence of Fe_3O_4 particles on the properties of PLA.

Experimental

Materials

A commercial PLA (trade name 6252D, about 6.86% D-isomer lactide) used for MB nonwoven processing was supplied by NatureWorks LLC (USA) and the melt index (MI) was about 120 g min^{-1} at 210 °C; Fe_3O_4 particle with a mean particle diameter of about 600 nm was provided by the Hebei Lingshou Mineral Powder Factory (China).

Preparation of PLA/Fe_3O_4 MB nonwoven

The melt-blowing process was performed in four steps. Prior to the processing, both PLA resins and Fe_3O_4 particles were dried in a vacuum oven at 80 °C for 12 h. After the mixture of PLA and Fe_3O_4 was mixed in the mass ratio of 100/0, 100/1, 100/3, and 100/5 by a mechanical mixer (SHR series high speed mixer, Giant company, Nanjing, China, rotate speed 1000 rpm), the PLA/Fe_3O_4 composites were prepared by feeding the mixture to a twin-screw extruder (TSE-30A, the ratio of length and diameter of the screw is 40 : 1, Nanjing Ruiya Extrusion System Co., Ltd, China) at 180 °C and 300 rpm; the composites with 0, 1, 3, 5 wt% content Fe_3O_4 were signed as C0, C1, C3, and C5, respectively. Finally, the composites were fed to a 45 cm wide research line with a single coat-hanger die (the diameter of each hole is 0.3 mm and the air-gap distance is 1.5 mm) melt-spun machine (Non-woven Research Laboratory of Zhejiang Sci-Tech University, Hangzhou, Zhejiang, China) to obtain the PLA/Fe_3O_4 MB nonwovens. The die temperature was in range of 200–230 °C and the temperature of hot air was 270 °C with a drawing air flow press of 0.08 MPa, 10 Hz metering pump frequency and a die to collector distance of 30 cm. The corresponding MB nonwovens were signed as M0, M1, M3, and M5. The preparation process of PLA/Fe_3O_4 nonwovens is shown in Fig. 1.

Characterization

Differential scanning calorimetry (DSC). The thermal properties of PLA/Fe_3O_4 composites were investigated by a DSC (DSC8000, Perkin-Elmer, US). All the samples were heated from 25 to 200 °C at 100 °C min^{-1} and maintained at 200 °C for 3 min to erase the previous thermal history, and then cooled down to 25 °C at 10°C min^{-1}. Finally, the samples were heated from 25 to 200 °C at 10°C min^{-1} once more to evaluate the second melting behavior and all experiments were performed under nitrogen atmosphere. It was obviously possible to obtain the glass transition temperature (T_g), the cold crystallization temperature (T_{cc}), the melt temperature (T_m), the cold crystallization enthalpy (ΔH_{cc}) and the melting enthalpy (ΔH_m) from the second heating curves of the samples. The relative degree of crystallinity (X_c) of all the samples was calculated using the equation, $X_c = \{(\Delta H_m - \Delta H_{cc}) \div \Delta H_o\} \times 100\%$, where ΔH_m and ΔH_{cc} were the melting enthalpy and the cold crystallization enthalpy of the samples respectively, ΔH_o was the fusion enthalpy of the completely crystalline PLA (the value taken as 93 J g^{-1} from literature),[31] and C was the weight fraction of PLA in the composites.

Wide-angle X-ray diffraction (XRD). The crystalline structure of PLA/Fe_3O_4 composites was evaluated by an X-ray diffractometer (D8 DISCOVERY, Bruker AXS, Geman) using a CuKα1 (=1.5406 Å) radiation source in the diffraction angle (2θ) range of 5–50° by steps of 5° min^{-1} at 40 kV and 40 mA. All the sample specimen dimensions were made approximately 1 × 40 × 40 mm (thickness–width–length) using the melt calendaring method at 190 °C, 10 MPa. Then, these plastic sheets were placed at room temperature for 48 hours before testing.

Thermogravimetric analysis (TGA). The thermal stability of PLA/Fe_3O_4 composites was studied on a TGA (TGA-Q50, TA Instruments, US) by scanning from 30 °C to 600 °C at a heating rate of 20°C min^{-1} under a nitrogen atmosphere.

Dynamic rheological measurements. The dynamic rheological behavior of PLA/Fe_3O_4 composites was determined by a Anton Paar Physica MCR 301 rheometer at 180 °C in the frequency scan range 0.1–400 rad s^{-1}. The measurements were performed in the linear viscoelastic region with dynamic oscillatory mode and 25 mm parallel cone-plate with gap setting of about 0.4 mm.

Scanning electron microscopy (SEM). The fracture surface morphology of the PLA/Fe_3O_4 composites and the surface morphology of the corresponding MB nonwovens were analyzed by scanning electron microscopy (SEM, ULTRA55, Carl Zeiss

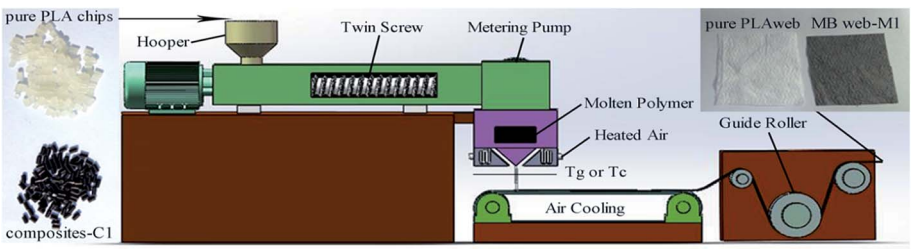

Fig. 1 The preparation process of PLA/Fe_3O_4 nonwovens.

AG, Germany) using a 3 kV accelerating voltage. Prior to the testing, the composite specimens were brittle fractured with liquid nitrogen, and all the composites and MB nonwoven samples were sputtered with gold to provide enhanced conductivity.

Magnetic property testing. A micro-vibration sample magnetometer (VSM 7407, Lakeshore, US) was used to measure the magnetic hysteresis loops of PLA/Fe_3O_4 MB nonwovens in the solid state at room temperature with an external 2 T magnetic field.

Filtration performance testing. The filtration efficiency of the PLA/Fe_3O_4 MB nonwovens was measured by an electron-laser particle spectrometer (WPS-1000xp, MSP Corp). The testing aerosol was sodium chloride (NaCl in the range of 0.3–0.5 μm) with 10 000 grains per m^3 at 5.3 cm s^{-1} velocity in air. The mass concentration of NaCl in the upstream volume (N_u) and the downstream volume of the air (N_d) was detected by an electron-laser particle spectrometer. The filtration efficiency (E) was calculated by the equation, $E = \{(N_u - N_d) \div N_u\} \times 100\%$. Five replicates were performed on each sample and the average values were recorded.

Result and discussion

Thermal properties of PLA/Fe_3O_4 composites

The second heating scanning curves of PLA/Fe_3O_4 composites were detected, as shown in Fig. 2a. Meanwhile, the glass transition temperature (T_g), cold crystallization temperature (T_{cc}), melt temperature (T_m) and relative crystallinity degree (X_c) of the samples determined from the DSC curves are summarized in Table 1. As seen from Table 1, T_g of pure PLA was about 61.5 °C, and T_g of all its composites were approximately 61 °C, suggesting that the addition of Fe_3O_4 had no significant change on the T_g of PLA. During the process of continuous heating, all the samples showed an exothermic peak corresponding to the cold crystallization process, which was caused by the mobility due to the rearrangement of PLA macromolecules. The relationship between T_{cc} and the content of Fe_3O_4 is plotted in Fig. 2b. Evidently, T_{cc} of the composites shifted to a higher temperature compared to neat PLA as the Fe_3O_4 content increased, which indicated that the Fe_3O_4 particles played an obvious hindrance for cold crystallization process of PLA.

Table 1 The related thermal results of PLA/Fe_3O_4 composites[a]

Sample	T_g (°C)	T_{cc} (°C)	T_{m1} (°C)	T_{m2} (°C)	X_c (%)
C0(PLA)	61.45	118.18	152.36	162.80	3.93
C1(PLA/Fe_3O_4-1)	61.49	123.19	154.96	164.61	1.15
C3(PLA/Fe_3O_4-3)	61.30	124.23	155.25	164.72	0.80
C5(PLA/Fe_3O_4-5)	61.17	124.57	155.32	164.74	0.78

[a] Data were summarized from the second heating cycles in DSC.

Moreover, the crystallinity degree of the composites decreased with the addition of Fe_3O_4. There were two aspects that might be taken into account to explain this phenomenon. On one side, Fe_3O_4 particles may disperse into the macromolecular chains, possibly disrupting the regularity of the PLA chain structure and hampering the crystallization process. On the other side, the concentration of Fe_3O_4 particles could act as blocking sites to hinder the growth of PLA crystallites through strengthening the molecular chain rigidity and decreasing the mobility, thus also resulting in a stronger impediment effect on the crystallization process.[32–34] All the samples had two distinct melting peaks; the mechanisms of dual (or multiple) lamellae population or crystal structure and melt-recrystallization could be used to explain the melting behavior of PLA.[35] The dual (or multiple) lamellae population or crystal structure mechanism considered the multiple melting with the different morphologies or crystal structures formed during the continue heating process, which may lead to the appearance of multiple melting peaks. In addition, the melt-recrystallization explanation suggests that the two separated peaks in the curves can be attributed to the melting of original crystals and the crystals re-formed through the melt-recrystallization process, and the crystallization of PLA at higher melting peak temperature were more perfect. Although the T_m of all the composites increased about 2 °C compared to neat PLA to some extent, the overall change was not notable and the T_m of all the samples were 164°.

Effect of Fe_3O_4 on the crystal structure

The XRD curves of Fe_3O_4 and PLA/Fe_3O_4 composites are illustrated in Fig. 3. Some research has been reported that the

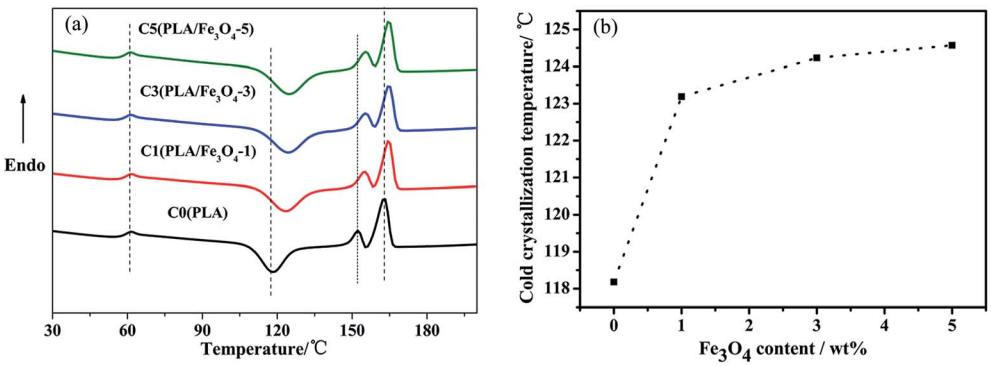

Fig. 2 (a) DSC curves of the second heating for PLA/Fe_3O_4 composites; (b) the cold crystallization temperature of the composites with different Fe_3O_4 content.

diffraction peaks of PLA homo-crystallites may exist at 2θ values of 16°, 18.4°, and 21.8°.[36] While our samples used for XRD test were obtained by melt calendaring method, it was difficult to form an ordered structure at 190 °C ($>T_m$). Moreover, the ability of the chain segment rearrangement cooled by air after melting to form crystals was limited due to the slow crystallization rate of PLA. Hence, a small and weak peak of pure PLA appeared at 2θ value of 16.8° corresponding to the (110) phase and the crystallinity was only 0.2%, indicating that neat PLA was almost amorphous. With the addition of Fe_3O_4, all the composites exhibited a wide angle diffraction peak of PLA, disclosing that the composites were also amorphous. The main peaks at 2θ values of 18.2°, 30.2°, and 35.4°, 43.1° seen from the XRD curve individually correspond to the (110), (220), (311), and (400) planes of Fe_3O_4, and all these peaks in the XRD pattern were indexed as face-centered cubic particles of Fe_3O_4 (JCPDS no. 16-0629); the average crystallite size of Fe_3O_4 particles was 31.1 (±0.9) nm, which was calculated from the Debye-Scherrer equation, $D = (K\lambda) \div \{\beta(2\theta) \times \cos\theta\}$, where $\beta(2\theta)$ was the full width at half-maximum (FWHM), K was a constant taken as the normal value of 0.9, and θ was the Bragg angle.[37] Obviously, the diffraction peak intensity of PLA in the composites did not increase with the increase in the content of Fe_3O_4; in contrast, all of them became smaller and wider. The reason may be that the addition of Fe_3O_4 hindered the arrangement of PLA molecular order and inhibited the formation of some PLA crystals, which was consistent with the result of DSC, but the crystalline structure of PLA had no change.

Effect of Fe_3O_4 on the thermal stability and dynamic rheological property

The TGA curves of PLA/Fe_3O_4 composites are plotted in Fig. 4. The decomposition temperature at 5 wt% and 50% weight loss (recorded as $T_{0.05}$ and $T_{0.50}$, respectively), the maximum decomposition temperature (T_{max}) and the remnant mass (the content of Fe_3O_4 can be calculated from the remnant mass) at the end of the curves at 600 °C are listed in Table 2. The weight loss curves of all the samples exhibited one simple thermal decomposition step within the temperature range of 280–390 °C. In fact, it was obviously observed that the temperature at 5 wt% weight loss of the composites, which can be used to evaluate the effect of Fe_3O_4 particles on the thermal stability,

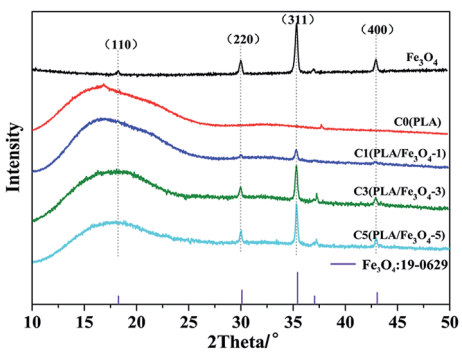

Fig. 3 XRD curves of Fe_3O_4, PLA and PLA/Fe_3O_4 composites.

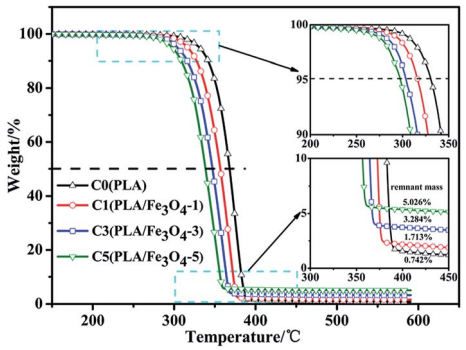

Fig. 4 TGA curves of pure PLA and the composites.

shifted downwards compared to neat PLA. This revealed that the thermal stability became worse with loading Fe_3O_4. It was possibly related to the adsorbed and absorbed water on the particles' surface; the active sites on their surface also could act as depolymerisation catalysts to accelerate the degradation of PLA.[38] All these factors may have caused the decrease in the molecular weight and promoted the degradation of PLA, which would reduce the viscosity of material under processing during a long time effect of heat and oxygen to some extent, it can be confirmed by the dynamic rheological curves shown in Fig. 5. It can be seen that all the samples demonstrated rather similar rheological properties, which exhibited non-newtonian shear thinning behaviors. However, the complex viscosity of all the composites was lower than that of pure PLA, and the phenomenon was more obvious with the addition of Fe_3O_4. Despite the addition of Fe_3O_4 accelerating the thermal degradation of PLA, it can still satisfy with the temperature window (185–240 °C) required for melt-blown processing.[39]

Morphology of PLA/Fe_3O_4 composites and MB nonwovens

The SEM micrographs of the fracture surface of PLA/Fe_3O_4 composites are shown in Fig. 6A and the morphology of PLA/Fe_3O_4 MB nonwovens in Fig. 6B. In fact, during the process, partly agglomerated particles could be effectively separated if they withstood a strong shear force during the mixture and polymer processing through the screw,[32] which could improve the dispersion of particles in the PLA phase to some extent. Hence, it can be seen that the particles were distributed homogeneously within the PLA matrix in the form of "sea-island" structure. Moreover, with the content of fillers increasing, the "sea-island" structure between Fe_3O_4 particles and PLA was clear, which showed the poor adhesion ability

Table 2 TGA results of PLA/Fe_3O_4 composites

Sample	$T_{0.05}$ (°C)	$T_{0.50}$ (°C)	T_{max} (°C)	Remnant mass (%)
C0(PLA)	331.35	367.46	392.89	0.74
C1(PLA/Fe_3O_4-1)	316.51	357.06	381.52	1.71
C3(PLA/Fe_3O_4-3)	303.50	346.66	370.77	3.28
C5(PLA/Fe_3O_4-5)	297.60	338.17	363.54	5.02

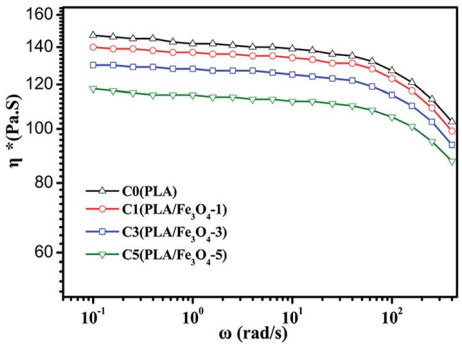

Fig. 5 Complex viscosity of PLA/Fe_3O_4 composites at 180 °C.

between PLA phase and Fe_3O_4 particles, leading to some big particles falling off from the polymer after been brittle fractured with liquid nitrogen and forming some holes. This phenomenon could be obviously observed with the high loading content of Fe_3O_4 particles (3 wt% and 5 wt%) according to Fig. 6A(c) and (d). While the fiber of pure PLA MB nonwoven prepared by melt-blowing processing using the PLA extrusion strip as the master batch was relatively uniform with a mean diameter of 0.6–1.5 μm, as shown in Fig. 6B(e), the fiber surfaces were sooth and the melt-blown web was dense. However, the fiber diameter of MB nonwovens became non-uniform and the web turned fluffy on loading Fe_3O_4 particles. Some Fe_3O_4 particles with the small size wrapped in the fibers during the melt blowing process; on the other hand, the larger particles were exposed on the surface of the fibers, which made the fiber surface become rough.

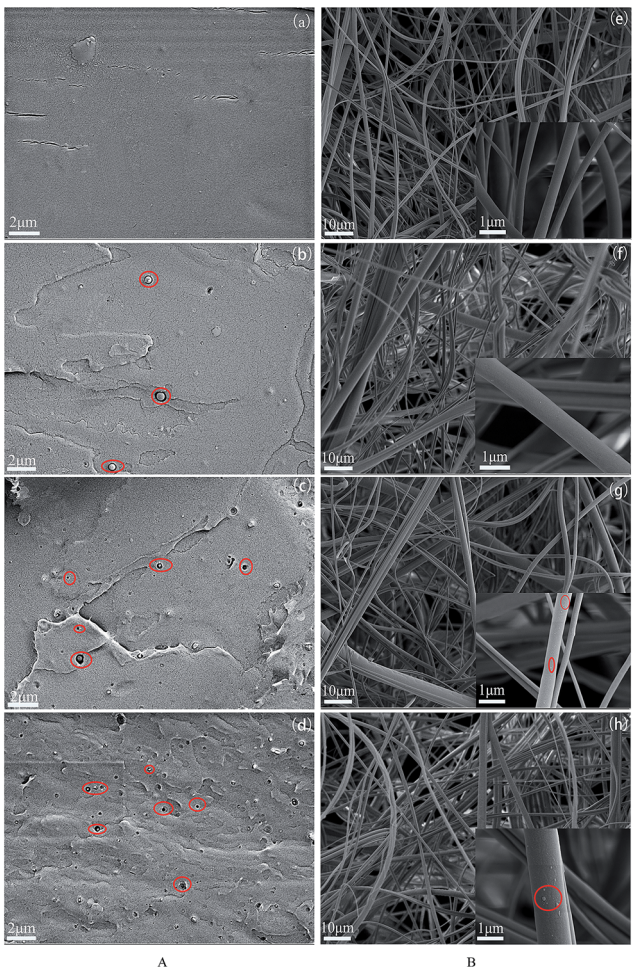

Fig. 6 (A) The fracture surface of PLA/Fe_3O_4 composites: (a) C0 (Pure PLA), (b) C1 (PLA/Fe_3O_4-1), (c) C3 (PLA/Fe_3O_4-3), (d) C5 (PLA/Fe_3O_4-5); (B) the morphology of the PLA/Fe_3O_4 MB nonwovens: (e) M0 (pure PLA), (f) M1 (PLA/Fe_3O_4-1), (g) M3 (PLA/Fe_3O_4-3), (h) M5 (PLA/Fe_3O_4-5).

Magnetic property analysis of PLA/Fe_3O_4 MB nonwovens

The magnetization hysteresis loops of PLA/Fe_3O_4 MB nonwovens are measured and shown in Fig. 7 to reveal their magnetic characterization. All the PLA/Fe_3O_4 MB nonwovens achieved their saturation magnetization (M_s), which was the maximum magnetization intensity corresponding to the value of the atom magnetic moment completely displayed in the same direction. With the addition of Fe_3O_4 particles increasing from 1 wt% to 5 wt%, the M_s of the MB nonwovens increased from 0.056 to 0.221 emu/g, while the M_s of pure PLA MB nonwoven was maintained at 0 because it had no magnetic response. The hysteresis curves showed that the PLA/Fe_3O_4 MB nonwovens had certain remanence (M_r) and coercivity (H_c). These values were small, which indicated that all the prepared PLA/Fe_3O_4 MB nonwovens were paramagnetic. It can be seen that the PLA/Fe_3O_4-1 MB nonwoven strip exhibited good magnetic response under the action of magnetic attraction; in contrast, there was no response of the pure PLA MB nonwoven strip. The MB nonwovens still owed certain magnetic response after the melt-blending and melt-blowing processing.

Filtration property of PLA/Fe_3O_4 MB nonwovens

Fig. 8 describes the filtration property of the pure PLA and the PLA/Fe_3O_4 MB nonwovens. Compared to the pure PLA MB nonwovens, the filtration efficiency of all the composite MB nonwovens increased from 42% to 68% as the content of Fe_3O_4 particles added increased from 0% to 5%. The morphology of PLA/Fe_3O_4 MB nonwovens indicated that the web turned fluffy and the fiber surface became rough on loading Fe_3O_4 powder,

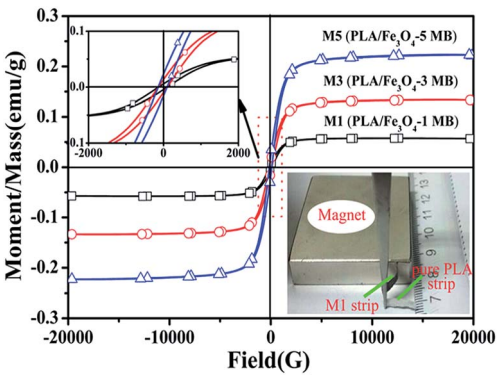

Fig. 7 The magnetization hysteresis loops of PLA/Fe_3O_4 MB nonwovens.

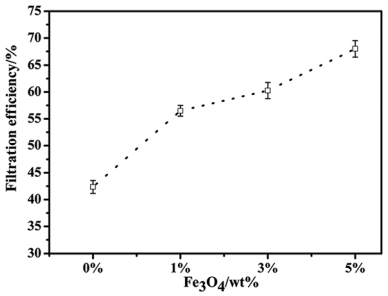

Fig. 8 The filtration efficiency curve of PLA/Fe_3O_4 MB nonwovens.

which could result in the testing particles getting impacted and captured more easily by the combined effects of sieving, diffusion, inertia and interception.[40] Moreover, the addition of Fe_3O_4 particles also affected the electrostatic and magnetic adsorption on some charged particles in air, which can also improve the filtration efficiency of the MB nonwovens.

Conclusion

In this study, PLA/Fe_3O_4 composites with different contents of magnetic Fe_3O_4 particles were prepared by melt-mixing process using a twin-screw extruder. Then, the MB nonwovens were obtained by melt blowing. Some measurements were conducted to evaluate the effect of magnetite on the composites and melt-blown materials in detail. The DSC results showed that Fe_3O_4 particles had an inhibition for the cold crystallization process of PLA, but the crystalline structure of PLA was unchanged. Though TGA and dynamic rheological measurements indicated the introduction of Fe_3O_4 reduced the thermal stability of the PLA, the decomposition temperature of the composites decreased as the content of Fe_3O_4 increases, it still could be satisfied with the temperature window required for melt-blowing process. According to the SEM observation, the Fe_3O_4 particles were uniformly dispersed in the PLA mixture in the form of the "sea-island" structure, and the particles also made the fiber surface become rough and the nonwoven web turned fluffy to some extent. Magnetic property and filtration performance testing on the MB nonwovens showed that the Fe_3O_4 particles not only endowed the PLA/Fe_3O_4 MB nonwovens with certain magnetic response after the melt-blending and melt-blowing processing a but also improved the filtration efficiency of PLA nonwovens, which showed a potential usage in the field of filter materials. This provided a method to develop functional PLA based composites, which can be applied in MB nonwoven materials for air filtration application. However, to obtain the PLA/Fe_3O_4 MB nonwovens with excellent performance, there were still some factors to be considered in the next works, such as the dispersion of Fe_3O_4, the compatibility between PLA matrix and Fe_3O_4 particles, and the different melt-blowing process condition.

Conflicts of interest

There are no conflicts to declare.

Acknowledgements

This work was financially supported by the Sci-Tech Plan Project of Zhejiang Province [Project No.: 2017C33077], the National Natural Science Foundation of China [grant number: 51203141] and 521 Talent Project of ZSTU.

References

1 M. A. Hassan, N. Anantharamaiah, S. A. Khan and B. Pourdeyhimi, *Ind. Eng. Chem. Res.*, 2016, **55**, 2049–2058.
2 C. J. Ellison, A. Phatak, D. W. Giles, C. W. Macosko and F. S. Bates, *Polymer*, 2007, **48**, 3306–3316.
3 A. K. Mohanty, M. Misra and L. T. Drzal, *J. Polym. Environ.*, 2002, **10**, 19–26.
4 T. Iwata, *Angew. Chem., Int. Ed.*, 2015, **54**, 3120–3215.
5 D. H. Muller and A. Krobjilowski, *Int. Nonwovens J.*, 2001, 11.
6 C. Liu, K. W. Chen, J. Shen, H. M. Wong, K. W. K. Yeung and S. C. Tjong, *RSC Adv.*, 2015, **5**, 72288–72299.
7 L. T. Lim, R. Auras and M. Rubino, *Prog. Polym. Sci.*, 2008, **33**, 820–852.
8 M. Jamshidian, E. A. Tehrany, M. Imran, M. Jacquot and S. Desobry, *Compr. Rev. Food Sci. Food Saf.*, 2010, **9**, 552–571.
9 B. Mallet, K. Lamnawar and A. Maazouz, *Polym. Eng. Sci.*, 2014, **54**, 840–857.
10 Y. Chen, L. M. Geever, J. A. Killion, J. G. Lyons, C. L. Higginbotham and D. M. Devine, *Polym.-Plast. Technol. Eng.*, 2016, **55**, 1057–1075.
11 V. H. Sangeetha, H. Deka, T. O. Varghese and S. K. Nayak, *Polym. Compos.*, 2016, DOI: 10.1002/pc.23906.
12 A. N. Frone, D. M. Panaitescu, I. Chiulan, C. A. Nicola, Z. Vuluga, C. Vitelaru and C. M. Damian, *J. Mater. Sci.*, 2016, **51**, 9771–9791.
13 Y. Liu, B. Cheng and G. Cheng, *Text. Res. J.*, 2010, **80**, 771–778.
14 B. Yu, J. Han, H. Sun, F. Zhu, Q. Zhang and J. Kong, *Polym. Compos.*, 2014, **36**, 264–271.
15 B. Yu, H. Sun, Y. Cao, J. Han, J. Kong, P. Wang and F. Zhu, *Polym.-Plast. Technol. Eng.*, 2014, **53**, 1788–1793.
16 I. H. Kim and Y. G. Jeong, *J. Polym. Sci., Part B: Polym. Phys.*, 2010, **48**, 850–858.
17 H. Liu, D. Bai, H. Bai, Q. Zhang and Q. Fu, *J. Mater. Chem. A*, 2015, **3**, 13835–13847.
18 C. Huang, H. Bai, H. Xiu, Q. Zhang and Q. Fu, *Compos. Sci. Technol.*, 2014, **102**, 20–27.
19 S. Davoodi, E. Oliaei, S. M. Davachi, I. Hejazi, J. Seyfi, B. S. Heidari and H. Ebrahimi, *RSC Adv.*, 2016, **6**, 39870–39882.
20 R. Scaffaro, L. Botta, A. Maio, M. C. Mistretta and F. P. L. Mantia, *Materials*, 2016, **9**, 351.
21 E. Picard, E. Espuche and R. Fulchiron, *Appl. Clay Sci.*, 2011, **53**, 58–65.
22 X. Jian, B. Wu, Y. Wei, S. Dou, X. Wang, W. He and N. Mahmood, *ACS Appl. Mater. Interfaces*, 2016, **8**, 6101–6109.
23 S. Ni, X. Sun, X. Wang, G. Zhou, F. Yang, J. Wang and D. He, *Mater. Chem. Phys.*, 2016, **124**, 353–358.

24 S. W. Bian, S. Liu and L. Chang, *J. Mater. Sci.*, 2016, **51**, 3643–3649.
25 L. He, L. Yao, F. Liu, B. Qin, R. Song and W. Huang, *J. Nanosci. Nanotechnol.*, 2010, **10**, 6348–6355.
26 J. Yang, P. Zou, L. Yang, J. Cao, Y. Sun, D. Han, S. Yang, Z. Wang, G. Chen, B. Wang and X. Kong, *Appl. Surf. Sci.*, 2014, **303**, 425–432.
27 N. Mhlanga, S. S. Ray, Y. Lemmer and J. Wesleysmith, *ACS Appl. Mater. Interfaces*, 2015, **7**, 22692–22701.
28 L. Hosseimi, K. Mahboobnia and M. Irani, *Int. J. Polym. Mater.*, 2016, **65**, 176–182.
29 H. Deng and Z. Lei, *Composites, Part B*, 2013, **54**, 194–199.
30 G. Lv, F. He, X. Wang, F. Gao, G. Zhang, T. Wang, H. Jiang, C. Wu, D. Guo, X. Li, B. Chen and Z. Gu, *Langmuir*, 2008, **24**, 2151–2156.
31 E. Fortunati, I. Armentano, Q. Zhou, D. Puglia, A. Terenzi, L. A. Berglund and J. M. Kenny, *Polym. Degrad. Stab.*, 2012, **97**, 2027–2036.
32 H. Zhang, J. Huang, L. Yang, R. Chen, W. Zou, X. Lin and J. Qu, *RSC Adv.*, 2015, **5**, 4639–4647.
33 Y. Sun and C. He, *ACS Macro Lett.*, 2012, **1**, 709–713.
34 D. Wu, Y. Cheng, S. Feng, Z. Yao and M. Zhang, *Ind. Eng. Chem. Res.*, 2013, **52**, 6731–6739.
35 P. Pan, W. Kai, B. Zhu, T. Dong and Y. Inoue, *Macromolecules*, 2007, **40**, 6898–6905.
36 X. Wei, R. Bao, Z. Cao, W. Yang, B. Xie and M. Yang, *Macromolecules*, 2014, **47**, 1439–1448.
37 D. Zhang, A. B. Karki, D. Rutman, D. Young, A. Wang, D. Cocke, T. H. Ho and Z. Guo, *Polymer*, 2009, **17**, 4189–4198.
38 C. Cifuentes, M. Lieblich, F. A. Lópeza, R. Benaventec and J. L. González-Carrascoa, *Mater. Sci. Eng., C*, 2017, **72**, 18–25.
39 J. M. Ferri, M. D. Samper, D. García-Sanoguera, M. J. Reig, O. Fenollar and R. Balart, *J. Mater. Sci.*, 2015, **51**, 5356–5366.
40 I. M. Hutten, *Handbook of Nonwoven Filter Media*, Elsevier, New York, 2007.